Appl. Phys. B 70, 361–366 (2000) / Digital Object Identifier (DOI) 10.1007/s003409900182

Applied Physics B
Lasers
and Optics

Influence of a feedback coupling on operating characteristics of a Cr^{3+}:$LiSrAlF_6$ laser using an end-coupled fiber grating

H. Parhat[1], **N.J. Vasa**[1], **M. Kidosaki**[1], **T. Okada**[1], **M. Maeda**[1], **T. Mizunami**[2], **O. Uchino**[3]

[1] Graduate School of Information Science and Electrical Engineering, Kyushu University, Fukuoka 812-8581, Japan
(Fax: +81-92/642-3969, E-mail: vasa@ed.kyushu-u.ac.jp)
[2] Department of Electrical Engineering, Kyushu Institute of Technology, Kitakyushu 804-8550, Japan
[3] Atmospheric Environment Division, Japan Meteorological Agency, Tokyo 100, Japan

Received: 23 April 1999/Revised version: 3 August 1999/Published online: 30 November 1999

Abstract. We describe a comparative study related to an influence of a feedback coupling on operating characteristics of a cw Cr^{3+}:$LiSrAlF_6$ (Cr^{3+}:LiSAF) laser using an end-coupled fiber grating with different coupling configurations. To achieve a compact construction, a direct butt-coupling of the fiber grating at the pump end of the Cr^{3+}:LiSAF laser and pumping through the same fiber was considered. The feedback provided by the coupled fiber grating through an end mirror was responsible for a spectrally narrowed output with a slope efficiency of 11%. However, the performance critically depended on an amount of the feedback coupling. The feedback-coupling condition was improved considerably by using a lens-coupled fiber grating at the pump end of the Cr^{3+}:LiSAF crystal. A spectrally narrowed output of $\approx 0.15\,cm^{-1}$ was obtained, and the output slope efficiency was measured as 27%. Theoretical modeling was also performed to understand the effect of the feedback coupling and the results agreed well with the experimental observations.

PACS: 42.55.R; 42.60B; 42.60D

Recently there has been a growing interest towards developing compact all-solid-state tunable Cr^{3+}:$LiSrAlF_6$ (Cr^{3+}:LiSAF) laser sources for high-resolution spectroscopic applications. A Cr^{3+}:LiSAF laser crystal has spectrally broad absorption and emission cross-sections with a fluorescence bandwidth extending from ≈ 750 to 1000 nm [1]. Further, this medium has a part of the broad absorption band (600–700 nm) matching with the commercially available InGaAlP red diode laser, which allows a compact assembly [2–5]. Since Cr^{3+}:LiSAF crystal is a low-gain laser material, as a simple approach for spectral narrowing and subsequent tuning operation, an externally coupled laser cavity with conventional tuning elements is preferred by many researchers [2, 6, 7]. This construction allows low insertion losses and hence a low threshold value.

In this respect, an approach of self-injection locking of the Cr^{3+}:LiSAF laser using an externally coupled fiber grating can also be considered for a compact and efficient operation. Single-mode tunable output has been reported using an externally coupled single-mode fiber grating at the output end of the Cr^{3+}:LiSAF laser. An output of 5 mW at an input of 200 mW (slope efficiency = 4.5%) was achieved [5]. Even though the spectral output could be improved, the slope efficiency was decreased due to decrease in the effective transmission as a result of partial feedback at the coupled-mode end. To improve the output characteristics, an application of the coupled fiber grating at the pump end of the Cr^{3+}:LiSAF laser crystal and providing the spectrally narrowed feedback through an end mirror instead of the output end can also be considered. In our previous experiments, pumping of the Cr^{3+}:LiSAF laser through different types of plain optical fiber without fiber grating was studied and the performance was analysed [8]. However, since plain fibers were used, the output was spectrally broad, and the analysis was limited to only the study of the spatial mode overlap as a function of the focusing conditions with a simple butt-coupled fiber configuration and without any feedback effect for the spectral narrowing operation. On the other hand, pumping of the Cr^{3+}:LiSAF laser through an optical fiber grating can provide dual advantages. It allows a more compact and efficient construction and a fiber grating formed on the same fiber acts as a part of the Cr^{3+}:LiSAFlaser coupled-cavity for self-injection locking and spectral-narrowing operation. However, the operating characteristics very much depend on the amount of a narrowband feedback coupling to the Cr^{3+}:LiSAF laser cavity.

In this work, different coupling configurations of a fiber grating at a pump end of a Cr^{3+}:LiSAF laser are considered and a comparative study is also made related to the influence of the feedback coupling on the spectral narrowing and output characteristics. In Sect. 1, a directly butt-coupled fiber grating configuration (BCFG) is considered for a very compact assembly with a minimum number of optical components and the influence of feedback coupling is studied. In Sect. 2, to improve the coupling of the narrowband feedback, a lens-coupled fiber grating configuration (LCFG) is investigated. The theoretical and experimental output characteristics including the feedback effect for both the configurations are described in Sect. 3 and finally the comparative study is summarized in Sect. 4.

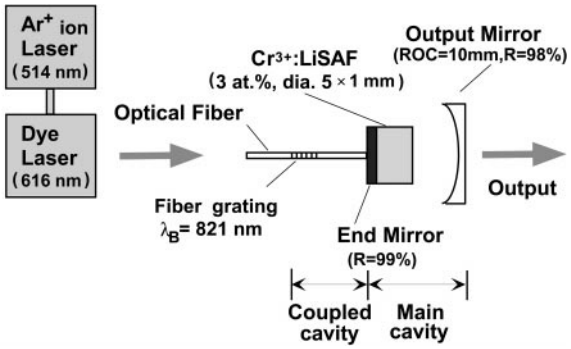

Fig. 1. Cr^{3+}:LiSAF laser with butt-coupled fiber grating (BCFG) configuration

1 Butt-coupled fiber grating (BCFG) configuration

1.1 Experiment

Figure 1 shows direct butt-coupling of a fiber grating configuration (BCFG) at the pump end of the Cr^{3+}:LiSAF crystal. It consisted of two parts, namely a main cavity and a coupled cavity. The main cavity was responsible for laser oscillation and the coupled cavity with a fiber grating provided a spectrally narrowband feedback for self-injection locking and the pumping was performed through the same butt-coupled fiber. The main cavity consisted of a plano-concave resonator arrangement with a 3 at. % doped Cr^{3+}:LiSAF crystal of 5 mm (diameter) × 1 mm (thickness). The crystal was coated for 99% reflectivity in the range from 800 to 900 nm on the pump-end face and antireflection-coated for the laser wavelength on the other face. An output coupler with a radius of curvature (ROC) 10 mm and reflectivity of 98% was used. We used a cw Ar^{+}-ion-laser-pumped Rhodamine 6G dye laser (616 nm), however, an AlGaInP red diode laser (670 nm) will be a practical source [9].

The fiber grating used in the auxiliary cavity was formed in a commercial germanosilicate multi-mode fiber (core diameter 9.3 μm, numerical aperture NA, 0.2) having a cutoff wavelength of 1300 nm. The reflection grating was generated in the H_2-loaded fiber by the side-writing holographic technique [10] similar to that described by Meltz et al. [11]. The length of the grating was 4 mm and the reflectivity was measured to be 65% at 821 nm with the linewidth of 0.45 nm FWHM. In the experiment, first a plain optical fiber without fiber grating was used and subsequently the fiber grating was applied to study the effect on spectral narrowing and output characteristics of the Cr^{3+}:LiSAF laser.

1.2 Spectral characteristics

The output of the Cr^{3+}:LiSAF laser pumped through the plain optical fiber was broadband with a peak around 830 nm and spectral width of ≈ 8 nm FWHM. When the optical fiber with fiber grating was used, spectral narrowing of the Cr^{3+}:LiSAF laser was observed, but it critically depended on the cavity length and the pump input power. Figure 2 shows the effect on spectral narrowing with respect to the cavity length of the Cr^{3+}:LiSAF laser and the pump input power.

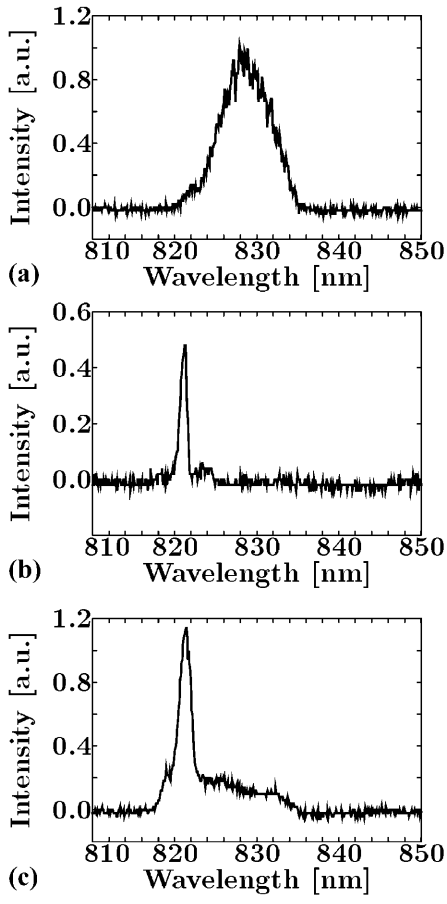

Fig. 2a–c. Spectral characteristics of Cr^{3+}:LiSAF laser with BCFG. **a** Cavity length $L_c \approx 9.5$ mm; **b** cavity length $L_c \approx 9.9$ mm, input pump power ≈ 60 mW; **c** cavity length $L_c \approx 9.9$ mm, pump input power ≈ 160 mW

Figure 2a shows the spectrum of the Cr^{3+}:LiSAF laser with the cavity length of around 9.5 mm where a maximum output was obtained. In this case, a small peak was observed near the Bragg wavelength (≈ 821 nm) of the fiber grating along with an unsuppressed broadband output. However with increase in the cavity length to 9.9 mm, quenching of the broadband output along with a spectrally narrowed output was observed as shown in Fig. 2b. In this case, the input pump power (≈ 60 mW) was near threshold requirement. However, when the input was increased to 160 mW, along with a spectrally narrowed peak around 821 nm, partially unsuppressed output near the high-gain modes was also observed as shown in Fig. 2c. When the spectral measurements were performed using a Fabry–Pérot interferometer, a multi-mode operation with two strong modes was observed. The free-spectral range of the Fabry–Pérot interferometer was ≈ 2 cm^{-1} and the measured spectral width was ≈ 0.7 cm^{-1}.

Next, a theoretical model was used to understand the effect of the feedback coupling on the spectral-narrowing operation. The feedback coupling includes a coupling of the laser mode with the fiber end and a coupling of a feedback mode with the laser mode. It depends on various loss mechanisms, such as coupling losses between the laser mode and the fiber end, coupling losses between the feedback mode and the laser mode distribution mismatch, the losses due to a positional and

angular mismatch of the fiber, and the reflection losses at the optics end. In the model, the amount of feedback coupling was calculated using a feedback-coupling factor η_c. Considering perfect alignment between the optical fiber end and the main cavity, and neglecting the reflectivity losses from the optics and the fiber end, the feedback-coupling factor η_c was described as

$$\eta_c = \alpha_m \alpha_f \,, \tag{1}$$

where α_m is the coupling coefficient due to the spatial matching between the Gaussian laser mode and the fiber core diameter (9.3 μm), and α_f is the coupling coefficient representing the spatial overlap between the top-hat feedback mode and Gaussian laser mode.

Figure 3 show plots of the theoretical value of the feedback-coupling factor η_c and a threshold ratio with respect to the cavity length L_c. In the plano-concave laser cavity, the laser mode size can be changed by altering the cavity length L_c. In Fig. 3, the feedback-coupling factor η_c was determined using (1), and the threshold ratio was defined as the ratio of the threshold pump power at free-running condition to the threshold pump power required during the feedback. Threshold pump power was determined based on the theoretical calculation described in Sect. 3. As shown in Fig. 3, with increase in the cavity length L_c the feedback-coupling factor η_c was improved. Therefore the threshold ratio was also increased and for a value greater than 1 spectral narrowing at the feedback mode could be expected. However, with decrease in the length of the laser cavity, the cavity mode size was increased compared to the fiber core size and the feedback-coupling factor η_c was decreased. Hence the threshold ratio was also decreased to a value less than 1, resulting in a high-gain free-running mode withholding spectral narrowing at the feedback mode. Further, from Fig. 3, even at large cavity length, the feedback-coupling factor η_c was not so high, and the resulting threshold ratio was very near to 1. Therefore complete quenching of the free-running mode was not possible at a high pump input, and along with a spectrally narrowed output, broadband free-running output could be expected. This critical effect was also observed during the experiment, as described in Fig. 2.

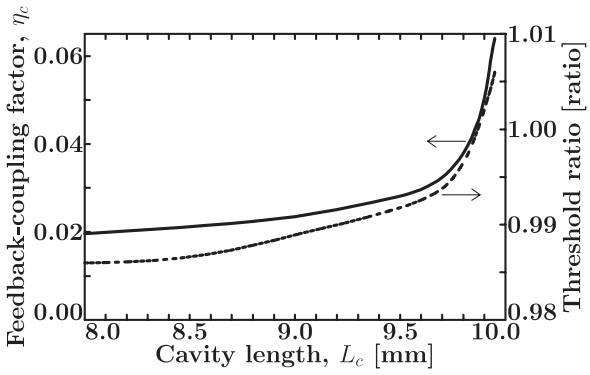

Fig. 3. Theoretical calculation of feedback-coupling factor η_c and threshold ratio with respect to cavity length L_c, for BCFG configuration. Threshold ratio is a ratio of the threshold power at free-running to the threshold power at feedback mode

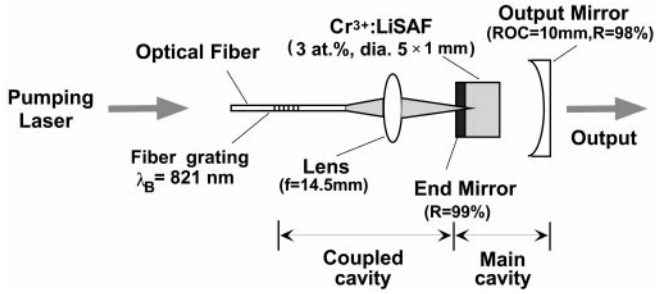

Fig. 4. Cr^{3+}:LiSAF laser with lens-coupled fiber grating (LCFG) configuration

2 Lens-coupled fiber grating (LCFG) configuration

2.1 Experiment

Subsequently, the laser performance of a lens-coupled fiber grating (LCFG) configuration was investigated. This construction was adopted to improve the feedback-coupling condition. Figure 4 shows the experimental arrangement. In this case, instead of a direct butt-coupling, the same optical fiber was coupled to the Cr^{3+}:LiSAF laser pump-end through a lens (Melles Griot, 06GLC003, $f = 14.5$ mm). The lens was located at around 18 mm from the fiber end and the crystal was located near the focused end of the lens. The lens position was near optimum with respect to the output characteristics and it was verified by the theoretical calculation described in Sect. 3. Subsequently, spectral narrowing operation and output characteristics were examined.

2.2 Spectral characteristics

Figure 5a,b show spectral characteristics of the Cr^{3+}:LiSAF laser with a cavity length of about 9 mm and with the input pump power of 150 mW. Figure 5a shows the free-running

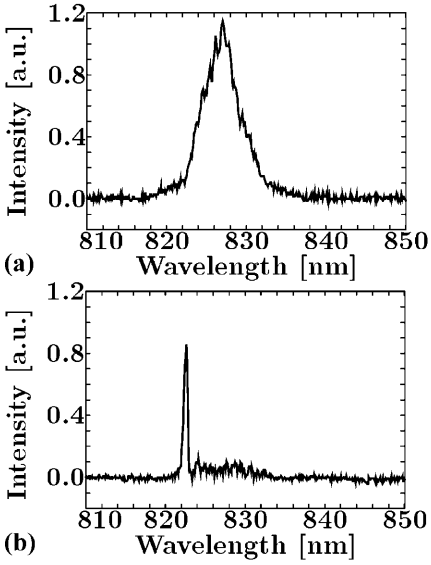

Fig. 5a,b. Spectral characteristics of Cr^{3+}:LiSAF laser with LCFG. Input pump power was ≈ 150 mW and cavity length L_c was ≈ 9 mm: **a** in free-running condition with lens-coupled plain fiber, **b** with fiber grating

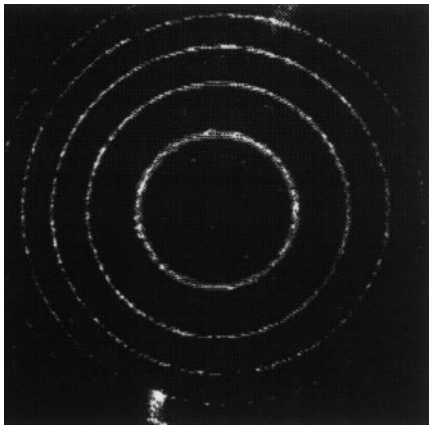

Fig. 6. Fabry–Pérot interference ring pattern of spectrally narrowed Cr^{3+}:LiSAF laser using LCFG. Spectral width was measured as 0.15 cm^{-1}. Free-spectral range was $\approx 2.5\,cm^{-1}$. The measurement was performed near threshold operation

spectrum of the Cr^{3+}:LiSAF laser when the plain fiber without fiber grating was used. The free-running output was broadband with a peak around 830 nm, and a spectral width of $\approx$ 7 nm FWHM. Figure 5b shows a spectrally narrowed output when the fiber grating was applied.

Figure 6 shows the Fabry–Pérot interference ring pattern of the spectrally narrowed Cr^{3+}:LiSAF laser output near threshold operation. The free-spectral range of the Fabry–Pérot interferometer was $\approx 2.5\,cm^{-1}$. The spectral width of the output was $\approx 0.15\,cm^{-1}$, and it was almost same even at a high input power. With the lens-coupled configuration also, the spectral-narrowing operation depended on the cavity length and effective narrowing could be obtained with the cavity length of around 9 mm. However, the operation was not as critical as in the case of the BCFG configuration.

Next, a theoretical study of the effect of the laser cavity length, and hence the effect of the laser mode size on the spectral narrowing was also made. Figure 7 shows plots of the feedback-coupling factor η_c and the threshold ratio with respect to the cavity length L_c. The feedback-coupling factor η_c was evaluated based on (1). Though its value depends upon the location of the coupling lens and focusing positions, in the calculations, the experimental location of the lens was used. As the cavity length L_c was increased, the feedback-coupling factor η_c and threshold ratio were also increased and after reaching a peak around the cavity length of 9.7 mm, the feedback-coupling factor η_c and threshold ratio were decreased. However, the threshold ratio in this range was greater than 1, representing lesser criticality in spectral-narrowing operation than the BCFG configuration. This was also confirmed experimentally and the alignment was also less sensitive as compared to the BCFG.

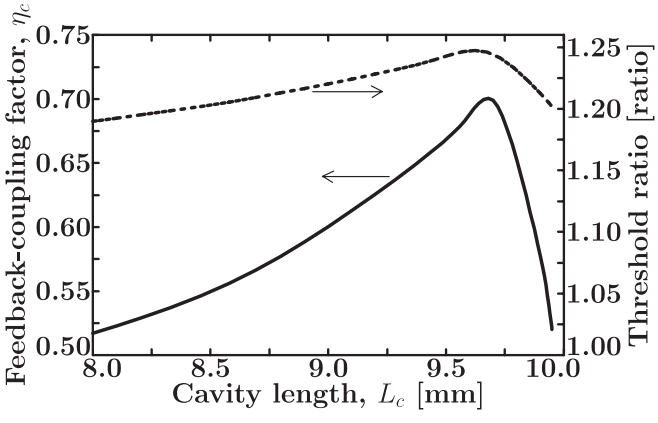

Fig. 7. Theoretical calculation of feedback-coupling factor η_c and threshold ratio with respect to the cavity length, for LCFG configuration. Threshold ratio is a ratio of the threshold power at free-running to the threshold power at feedback mode

3 Output characteristics

3.1 Theoretical model

In the case of a conventional straight cavity configuration, based on the space-dependent rate equation analysis, the threshold power requirement and the relationship between an input and output power has been investigated by several authors [12, 13]. This model can be extended to the fiber grating coupled-cavity configurations with some modifications related to the pumping charcateristics and the feedback effect from the fiber grating. Based on a space-dependent rate equation analysis, the threshold power P_{th} can be estimated by

$$P_{th} = \frac{\sigma_e \gamma\, I_s}{2\eta_p(\sigma_e - \sigma_{esa})} \frac{1}{\int_{cavity} gm\, dV}\,, \tag{2}$$

where σ_e is the stimulated emission cross section, γ is the total logarithmic loss ($2\alpha_c l + T_{out} - \ln(1/R_{eff})$, α_c is the distributed loss per unit length, l is the crystal length, T_{out} is the transmission loss at the output mirror, R_{eff} is the effective reflectivity of the end mirror considering the feedback, η_p is the pump efficiency (ν_l/ν_p), ν_l is and ν_p are the laser and pump frequencies respectively, σ_{esa} represents loss in the gain cross-section due to excited state absorption (ESA), I_s is the saturation intensity ($h\nu_l/\sigma_e\tau$), $h\nu_l$ is the energy of the laser photon, τ is the upper-state lifetime, g and m represents normalized pump and normalized laser mode distributions inside the active medium, respectively, and $\int_{cavity} gm\,dV$ represents effective spatial overlapping of the pump and laser mode distributions. In this case, the pump beam distribution is considered to be a top-hat distribution [14, 15].

The feedback effect from the coupled fiber grating can be included as follows. In the coupled-cavity configuration, the effective reflectivity R_{eff} for the feedback mode can be calculated based on a simple electric wave model and considering a Fabry–Pérot cavity construction between the end mirror of the Cr^{3+}:LiSAF laser and the coupled fiber grating. Assuming a perfectly resonant external cavity for the coupled mode, and considering the feedback-coupling factor η_c for the coupling losses of the coupled cavity per transit, the effective reflection R_{eff} can be expressed as

$$R_{eff} = \left[\frac{r_{end} + \eta_c r_{fiber}}{1 + r_{end}\eta_c r_{fiber}}\right]^2\,, \tag{3}$$

where r_{end} is the reflective coefficient of the end mirror ($r_{end} = \sqrt{R_{end}}$), r_{fiber} is the reflective coefficient of the fiber grating ($r_{fiber} = \sqrt{R_{fiber}}$).

Table 1. Standard parameter values used in theoretical calculations

Description	Symbol	Numerical values
Pump wavelength	λ_p	616 nm
Laser wavelength	λ_c	821 nm
Absorption coefficient	α_p	14 cm^{-1}
Fluorescence lifetime	τ	67 μs
Refractive index — at λ_p	n_p	1.4094
Refractive index — at λ_c	n_c	1.4076
Free-running at 830 nm		
– Stimulated-emission cross-section	σ_e	4.9×10^{-20} cm^2
– ESA cross-section	σ_{esa}	1.8×10^{-20} cm^2
Feedback at 821 nm		
– Stimulated-emission cross-section	σ_e	4.77×10^{-20} cm^2
– ESA cross section	σ_{esa}	1.7×10^{-20} cm^2
Distributed loss per unit length	α_c	0.015 cm^{-1}
End mirror reflectivity	R_{end}	0.99
Output mirror reflectivity	R_{out}	0.98

Finally, the modified output characteristics can be given by

$$P_{out} = \frac{T_{out}\eta_p}{\gamma}\frac{(\sigma_e - \sigma_{esa})}{\sigma_e}[P_{in} - P_{th}]\frac{\left[\int_{cavity} gm \, dV\right]^2}{\int_{cavity} gm^2 \, dV}, \qquad (4)$$

where P_{out} is the laser output power, $(\int_{cavity} gm \, dV)^2 / \int_{cavity} gm^2 \, dV$ represents a factor affecting an overlapping efficiency and it is termed as a mode-coupling factor (mcf). Thus the slope efficiency, η_s, is the product of a coupling efficiency T_{out}/γ, pump efficiency η_p, a factor due to excited-state absorption $(\sigma_e - \sigma_{esa})/\sigma_e$, and the mode-coupling factor mcf.

Subsequently, the integrations in (2) and (4) were solved numerically to yield the theoretical output characteristics for the BCFG and LCFG configurations. The mathematical analyses were simplified further by considering a collinear pump and laser mode beam geometry in the gain medium. The theoretical calculations were performed using the values of the standard parameters described in Table 1.

3.2 Results

Figure 8 shows theoretical and experimental output characteristics of the Cr^{3+}:LiSAF laser with the BCFG and LCFG configurarions. The solid line represents theoretical output characteristics and the solid circles represent experimental output characteristics of the BCFG configuration. The experimental threshold pump power was measured as 45 mW. A good fit between the experiment and the theory was obtained corresponding to the feedback-coupling factor $\eta_c \approx 0.03$, and the effective reflectivity $R_{eff} \approx 0.9904$. In this case the cavity length was considered to be 9.9 mm, the same as in the experiment. Based on theoretical fitting, the threshold pump power was 49 mW and the slope efficiency η_s was estimated to be 11%.

The dotted line and hollow circles in Fig. 8 represent theoretical and experimental output characteristics of the LCFG configuration, respectively. The experimental threshold pump power was measured as 77 mW. Theoretical fitting was obtained with the feedback-coupling factor $\eta_c \approx 0.5$, and the corresponding effective reflectivity $R_{eff} \approx 0.995$. In this case

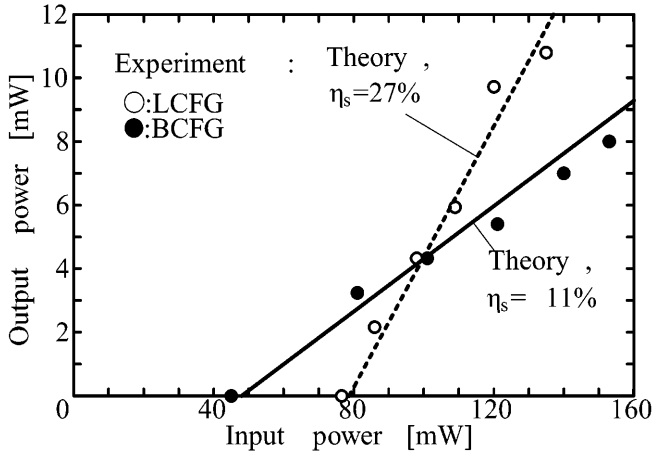

Fig. 8. Output characteristics of Cr^{3+}:LiSAF laser with coupled fiber grating. *Solid line* represents theoretical output characteristics and *solid circles* represent experimental output characteristics of BCFG configuration. *Dotted line* represents theoretical output characteristics and *hollow circles* represent experimental output characteristics of LCFG configuration

the cavity length was considered to be 9 mm, the same as in the experiment. The threshold pump power was 79 mW and the slope efficiency η_s was estimated to be 27%. With a lens-coupled plain fiber without fiber grating, the experimental threshold pump power was increased to 98 mW. Based on the theoretical fitting, the slope efficiency η_s was estimated to be 22.8%, and as expected it was less than the LCFG configuration.

In both the configurations, the estimated values of the feedback-coupling factor η_c based on the theoretical fitting were less than the theoretical values calculated from (1). This can be attributed to the losses due to fiber misalignment which were not taken into account during the theoretical calculations. Nevertheless, it is worthwhile to note that, with an improvement in the feedback-coupling factor ($\eta_c = 0.6$) for the LCFG configuration, and using the fiber grating with the maximum possible reflectivity of 1, the effective reflectivity R_{eff} for the feedback operation is expected to be increased to 0.9974. In turn, the theoretical threshold power will decrease to 73 mW and the slope efficiency η_s will be 29%. Further, we also expect that by using the LCFG configuration with a micro-lens at the fiber end, a spectrally narrowed, microchip Cr^{3+}:LiSAF laser can also be attained. This configuration can also be applied to other tunable microchip lasers without any intracavity tunable elements for a spectrally narrowed output, such as waveguided Ti:sapphire lasers with an externally coupled fiber grating at the pump end. Even though, a wide tuning range can not be achieved by using the fiber grating, the required wavelength can easily be obtained by proper selection of a desired fiber grating and subsequent temperature or tension tuning.

4 Conclusions

The influence of feedback coupling on the performance of the Cr^{3+}:LiSAFlaser pumped through the fiber grating with two different schemes, namely, directly butt-coupled (BCFG) configuration, and lens-coupled (LCFG) configuration was

investigated. The main attractive feature of the BCFG configuration is the compactness and simplicity in the construction. In the BCFG, the slope efficiency η_s of $\approx 11\%$ was obtained and the spectral narrowing critically depended on the feedback-coupling condition. The experimental and theoretical study show that there is a limitation in feedback coupling due to the laser mode size and fiber core size matching condition. A larger core diameter fiber can be considered for improving the feedback coupling, however the slope efficiency will decrease due to increase in the pump beam spot size. Therefore, there exists a trade-off between obtaining a high slope efficiency and obtaining an effective spectral narrowing. By using a higher reflectivity fiber grating, as well as reducing the feedback mode coupling losses, the performance is expected to be improved to some extent.

Compared to the BCFG, the LCFG provided a better self-injection locking operation even though the construction involved an extra focusing lens. The feedback coupling theory clearly explained the advantage of the scheme. The slope efficiency η_s of $\approx 27\%$ was achieved and the spectrally narrowed ($\approx 0.15\,\mathrm{cm}^{-1}$) output was obtained even at high pump input. The spectral narrowing is expected to be improved further by increasing the reflectivity of the fiber grating and improving the feedback coupling. This configuration is the best suited for spectrally narrowed output characteristics. This technique can also be applied for designing any other laser system when pumped through a coupled fiber grating.

Acknowledgements. The authors would like to thank Prof. K. Uchino of Interdisciplinary Graduate School of Engineering Sciences, Kyushu University, for extending the argon-ion laser facility for the experiment.

References

1. M. Stalder, B.H.T. Chai, M. Bass: Appl. Phys. Lett. **58**, 216 (1991)
2. Q. Zhang, G.J. Dixon, B.H.T. Chai, P.N. Kean: Opt. Lett. **17**, 43 (1992)
3. J.M. Sutherland, S. Ruan, R. Mellish, P.M.W. French, J.R. Taylor: Opt. Commun.**113**, 458 (1995)
4. R. Knappe, K.J. Boller, R. Wallenstein: Opt. Lett. **20**, 1988 (1995)
5. N.J. Vasa, T. Okada, M. Maeda, T. Mizunami, O. Uchino: Opt. Lett. **21**, 1472 (1996)
6. N.J. Vasa, H. Sui, H. Parhat, T. Okada, M. Maeda, O. Uchino: Jpn. J. Appl. Phys. **35**, 4369 (1996)
7. M. Tsunekane, M. Ihara, N. Taguchi, H. Inaba: IEEE J. Quantum Electron. **QE-34**, 1288 (1998)
8. N.J. Vasa, H. Parhat, T. Okada, M. Maeda, O. Uchino: Opt. Commun. **147**, 196 (1998)
9. R. Schep, J.F. Myers, H.B. Serreze, A. Rosenberg, R.C. Morris, M. Long: Opt. Lett. **16**, 820 (1991)
10. T. Mizunami, S. Gupta, T. Yamao, T. Shimomura: International Conference on Integrated Optics and Optical Fiber Communications/23rd European Conference on Optical Communications, UK **3**, 182 (1997)
11. G. Meltz, W.W. Morey, W.H. Glenn: Opt. Lett. **14**, 823 (1989)
12. A.J. Alfrey: IEEE J. Quantum Electron. **QE-25**, 760 (1989)
13. P. Laporta: IEEE J. Quantum Electron. **QE-27**, 2319 (1991)
14. Y.F. Chen, T.S. Liao, C.F. Kato, T.M. Huang, K.H. Lin, S.C.Wang: IEEE J. Quantum Electron. **32**, 2010 (1996)
15. Y.F. Chen, C.F. Kao, S.C. Wang: Opt. Commun. **133**, 517 (1997)